Examining the Modular Synthesis of [Cp*Rh] Monohydrides Supported by Chelating Diphosphine Ligands

Chelsea G. Comadoll,[a] Wade C. Henke,[a] Julie A. Hopkins Leseberg,[a] Justin T. Douglas,[b] Allen G. Oliver,[c] Victor W. Day,[a] and James D. Blakemore*,[a]

[a] Department of Chemistry, University of Kansas, 1567 Irving Hill Road, Lawrence, Kansas 66045, United States

[b] Nuclear Magnetic Resonance Laboratory, Molecular Structures Group, University of Kansas, 2034 Becker Drive, Lawrence, Kansas 66047, United States

[c] Department of Chemistry and Biochemistry, University of Notre Dame, 149 Stepan Chemistry, Notre Dame, Indiana 46556, United States

Supporting Information Placeholder

ABSTRACT: [Cp*Rh] hydride complexes are invoked as intermediates in certain catalytic cycles, but few of these species have been successfully prepared and isolated, contributing to a relative shortage of information on the properties of such species. Here, the synthesis, isolation, and characterization of two new [Cp*Rh] hydrides are reported; the hydrides are supported by the chelating diphosphine ligands bis(diphenylphosphino)methane (dppm) and 4,5-bis(diphenylphosphino)-9,9-dimethylxanthene (Xantphos). In both systems, reduction of precursor Rh(III) chloride complexes with Na(Hg) results in clean formation of isolable, formally 18e$^-$ Rh(I) species, and subsequent protonation by addition of near-stoichiometric quantities of anilinium triflate to the Rh(I) species returns high yields of the desired monohydride complexes. Single-crystal X-ray diffraction data for these compounds provide evidence of direct Rh–H interactions, confirmed by complementary infrared spectra showing Rh–H stretching frequencies at 1982 cm^{-1} (for the dppm-supported hydride) and 1936 cm^{-1} (for the Xantphos-supported hydride). Findings from comprehensive multinuclear NMR experiments reveal the properties of the unique and especially rich spin systems for the dppm-supported hydride; multifrequency NMR studies in concert with spectral simulations enabled full characterization of splitting patterns attributable to couplings involving diastereotopic methylene protons for this complex. Taken together with prior reports of related monohydrides, the results show that the reduction/protonation reaction sequence is modular for preparation of [Cp*Rh] monohydrides supported by diverse diphosphine ligands spanning from four- to eight-membered rhodacycles.

INTRODUCTION

Metal hydrides are an important class of compounds in organometallic chemistry, serving as key intermediates in a variety of catalytic processes.[1] Attention is often paid to these species for their high relevance to electrocatalysis as well, in that metal-mediated production of H_2 from H_2O and reduction of CO_2 often involve metal hydride intermediates generated under reductive conditions.[2]

One such catalytic system that has attracted significant attention is the generation of H_2 by [Cp*Rh] complexes (where Cp* is η^5-pentamethylcyclopentadienyl) supported by the workhorse 2,2′-bipyridyl ligand (bpy) and its analogues.[3] This system is readily prepared from common ligands and the useful precursor $[Cp^*RhCl_2]_2$,[4] and can operate both chemically and electrochemically.[5] Mechanistically, the catalyst supported by bpy undergoes a two-electron reduction followed by protonation;[6] such a reaction sequence has conventionally been discussed to yield a [Cp*Rh] monohydride that could undergo protonolysis to generate H_2 and close the catalytic cycle. The same hydride intermediate has also been proposed to be involved in generation of NADH from NAD^+ in related bioelectrochemical work, magnifying its importance on this platform.[7]

The [Cp*Rh] hydride supported by bpy has a central role in the chemistry of this system, but so far, this species has eluded isolation or full characterization. In part, this is due to formation of favored η^4-pentamethylcyclopentadiene (Cp*H) complexes under some conditions; on the other hand, the precise relationship of the Cp*H complexes to the catalytic mechanism is not yet fully mapped.[8] Notably, signals attributable to a hydride species have been observed upon treatment of a [Cp*Rh] complex supported by 6,6′-dimethyl-2,2′-bipyridyl with excess sodium formate under stringent reaction conditions.[9] Similarly, hydride signals have been observed in low temperature nuclear magnetic resonance (NMR) spectroscopy experiments with the bpy system in the presence of strong acid (HCl, pK_a < 10 in MeCN).[10] And, the analogous [Cp*Ir] hydride is well known and has been crystallographically characterized,[11] lending credence to proposals for involvement of [Cp*Rh] monohydrides in these systems.

In light of the probable involvement of transient hydride complexes in the chemistry of [Cp*Rh] catalysts, we have recently been developing synthetic routes to access model [Cp*Rh] monohydrides in order to study their chemical properties. In prior work, we have prepared and isolated two monomeric [Cp*Rh] hydride complexes bearing the ligands (diphenylphosphino)quinoline (pqn)[12] and bis(diphenylphosphino)benzene (dppb)[13] (**H** and **B**, respectively, see Chart 1). These hydrides are remarkably resistant to further reactivity upon preparation, with cleavage of the Rh–H bond via

protonolysis being disfavored in the presence of excess anilinium triflate (pK_a = 10.6 in MeCN[14]). Although **H** does evolve hydrogen in the presence of stronger acids, **B** does not; this finding is consistent with prior literature reports which have shown that metal hydride complexes are stabilized by phosphine ligands.[15,16]

Chart 1. [Cp*Rh] hydride species supported by bidentate chelating ligands. Rhodium is in the formally +III oxidation state in all cases.

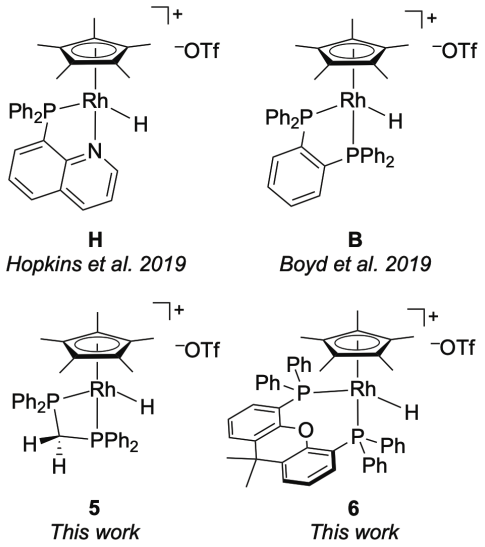

Isolation of hydride species **H** and **B** enabled thorough characterization of the compounds in both cases and provided new insights into the chemistry of the parent catalytic system. However, these two cases represent disparate examples of hydride generation on the [Cp*Rh] platform via a common sequential reduction/protonation pathway. This reaction sequence is directly relevant to chemical and electrochemical use of these complexes and thus is deserving of further scrutiny; most applications of these compounds rely on the air-stable Rh(III) complexes as starting materials, and thus reduction and protonation can be identified as critical steps in the chemistry of these compounds.[17] In this context, significant prior work across many platforms has shown that the tuning of phosphine ligands can induce significant structural and electronic changes to the corresponding metal complexes. We anticipated here that examination of the modularity of the reduction/protonation reaction sequence on the [Cp*Rh] platform across varying κ^2-diphosphine ligands could provide new details on factors that enable clean generation of [Cp*Rh] monohydride species, as well as reveal the impact of changing rhodacycle size on the structure and reactivity of [Cp*Rh] hydrides.

Here, we report the synthesis and full characterization of two new [Cp*Rh] monohydride complexes supported by the chelating diphosphine ligands bis(diphenylphosphino)methane (dppm) and 4,5-bis(diphenylphosphino)-9,9-dimethylxanthene (Xantphos). The synthetic chemistry is modular for both systems and affords good yields for all three steps involved (preparation of the Rh(III) precursor, reduction, and protonation, respectively; each step ≥ 80 %). All six of the complexes involved here were characterized by NMR techniques as well as single-crystal X-ray crystallographic analysis, highlighting the distinctive four- and eight-membered rhodacycles present in the dppm and Xantphos systems, respectively. The dppm complexes display uncommonly rich NMR spectral properties, which were elucidated through both multifrequency experiments (spanning 400 to 800 MHz) and related digital simulations. Taken together with prior work, our findings show that [Cp*Rh] complexes ligated by a variety of diphosphine ligands display remarkably clean and modular reactivity toward the generation of Rh–H species.

RESULTS AND DISCUSSION

Synthesis and Characterization of the Bis(phosphino) Complexes. We have previously found that the dimeric complex $[Cp^*RhCl_2]_2$, developed by Maitlis and co-workers,[4] is a reliable synthetic precursor to a variety of [Cp*Rh] complexes. Using this material, we developed a synthetic route for the preparation and isolation of a monomeric [Cp*Rh] hydride complex **B** which relies on a sequential redox chemistry approach.[13] In this procedure, initial preparation of a rhodium(III) complex is followed by reduction to a formally rhodium(I) intermediate. We found that this rhodium(I) form could undergo clean protonation to a rhodium(III) hydride, contrasting with recent findings for diimine-type ligands in which exposure of the reduced form to acid results in protonation of the η^5-Cp* ligand.[5] In order to investigate the modularity of the synthetic route developed for **B**, we explored similar methods here for the synthesis of [Cp*Rh] complexes bearing the related diphosphine ligands dppm and Xantphos (Scheme 1), which differ from dppb in that they commonly form four- and eight-membered rhodacycles, respectively, in contrast with the five-membered rhodacycle of **B**.

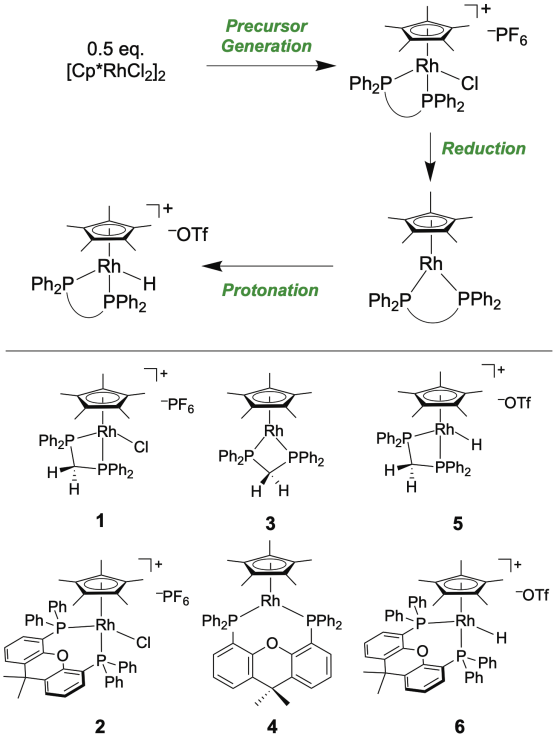

Scheme 1. Preparation of Cp*Rh complexes. Upper panel: Synthetic strategy using sequential reduction/protonation. Lower panel: Structures of the compounds described in this work.

To begin, we reacted 0.5 equivalents of $[Cp^*RhCl_2]_2$ with 1.0 equivalent of $AgPF_6$, followed by the addition of 1.05 equivalents of dppm or Xantphos, giving good yields of **1** and **2** (see Scheme 1) as

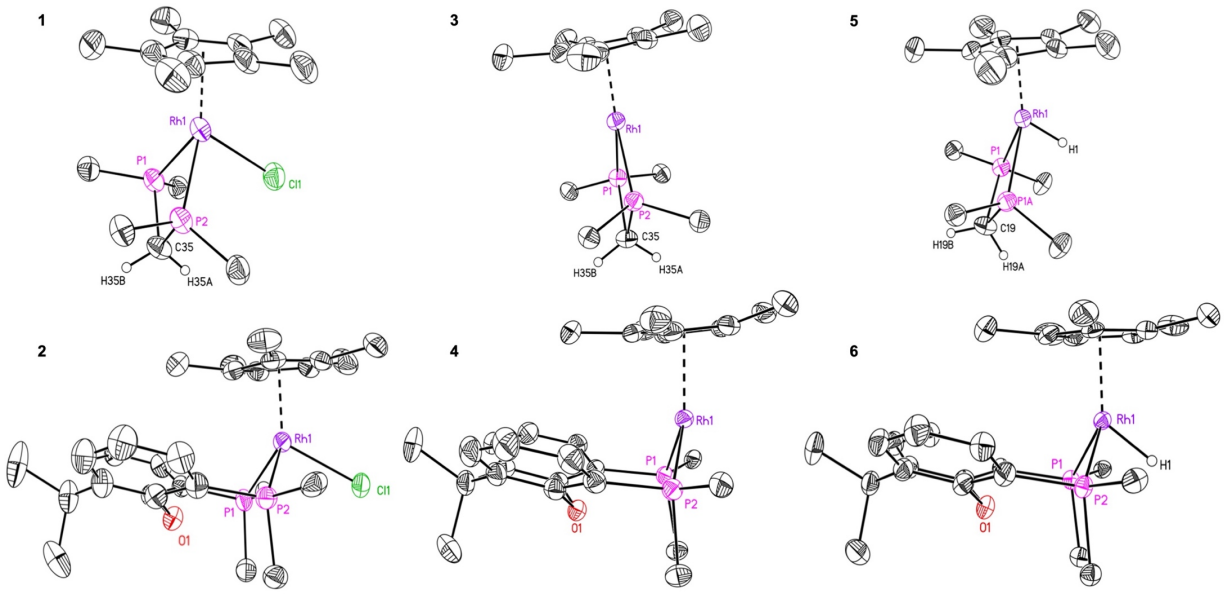

Figure 1. Solid-state structures of the [Cp*Rh] complexes reported in this work. Left column: chloride complexes with formal Rh(III) oxidation state; **1** (upper), **2** (lower). Middle column: reduced complexes with formal Rh(I) oxidation state; **3** (upper), **4** (lower). Right column: monohydride complexes with formal Rh(III) oxidation state; **5** (upper), **6** (lower). Displacement ellipsoids are shown at the 50% probability level. Phenyl rings, hydrogen atoms (except H35A, H35B, H19A, H19B, and H1), outer sphere counteranions, and co-crystallized solvent molecules are omitted for clarity.

yellow and orange air-stable solids, respectively. Notably, preparation of **1** has been reported previously by two groups; the Tatsumi group isolated **1** as a byproduct (in 26 % yield) in the context of a synthetic route targeting alkenylated [Cp*Rh] species,[18a] whereas the Nakajima group reported preparation of **1** (in 80 % yield) so that it could be used as a reference compound.[18b] However, neither group reported full characterization, crystallographic analysis, or reactivity studies for **1**, as the chemistry of the compound was incidental to their work in both cases. Here, full spectroscopic confirmation of the formulations of **1** and **2** came from ^{1}H NMR. All NMR spectral data for **1** and **2** can be found in the Supporting Information (SI, Figures S1–S10). For both **1** and **2**, a triplet integrating to 15 protons is present at 1.74 and 0.97 ppm, respectively, representing the equivalent Cp* methyl protons. The peak is a triplet in both cases due to coupling to the chelating phosphorus atoms ($^{4}J_{H,P}$ = 4.1 Hz for both **1** and **2**). Additionally, the ^{31}P{^{1}H} NMR spectra of both complexes reveal a septet representing the PF_6^- counterion, along with a doublet corresponding to the respective diphosphine ligand which couples to rhodium ($^{1}J_{P,Rh}$ = 115.1 Hz, 143.4 Hz for **1** and **2**, respectively).

Interestingly, the ^{1}H spectrum of **1** shows two distinct and unique sets of resonances centered at 4.91 ppm (dtd) and 4.51 ppm (dt) belonging to the diastereotopic methylene protons on the backbone of the dppm ligand (δ = 4.91 ppm, dtd, $^{2}J_{H,H}$ = 15.6 Hz, $^{2}J_{H,P}$ = 10.1 Hz, $^{3}J_{H,Rh}$ = 1.7 Hz; δ = 4.51 ppm, dt, $^{2}J_{H,H}$ = 15.6 Hz, $^{2}J_{H,P}$ = 13.0 Hz). The difference in the splitting pattern between these two protons arises as a result of their distinct chemical and magnetic environments, as well as the overall rich nuclear spin system of the complex. While both methylene protons couple to the two phosphorus atoms, the more upfield of the two couples more strongly to phosphorus. Seemingly in contradiction with this observation, only the other, more downfield methylene proton couples to rhodium. This difference between these observed couplings is likely attributable to geometric differences between the two protons in solution, because their positions with respect to the phosphorus atoms and rhodium center in the solid state are similar (*vide infra*). Likewise, the ^{1}H NMR spectrum of **2** displays two singlets at 2.00 and 1.68 ppm, representing the diastereotopic geminal methyl groups on the Xantphos ligand. However, as expected, these singlets contrast with the intricate splitting observed for the diastereotopic methylene protons of the dppm framework.

Vapor diffusion of diethyl ether into a concentrated acetonitrile solution of **1** or an acetone solution of **2** afforded orange and red crystals, respectively, that were suitable for X-ray diffraction (XRD) studies. Details on the crystallographic work can be found in the SI (pp. S26–S48). The solid-state structures reveal the geometries around the formally Rh(III) centers to be *pseudo*-octahedral in both cases (see Figure 1). Each rhodium center has a first coordination sphere containing the [η^5-Cp*] ligand, the expected κ^2-diphosphine ligand, and a single chloride ligand. The bond metrics for **1** and **2** show, as could be anticipated, that the Rh–P bond lengths are longer in **2** than they are in **1**; this is attributed to the larger, more distorted eight-membered rhodacycle present in **2** (see Table 1). The P1–Rh–P2 angles of the diphosphine ligands also reflect this situation, as use of dppm results in a much tighter bite angle for **1** of 72.20(5)° relative to 95.38(3)°/95.69(3)° for Xantphos in **2**. On the other hand, we also found the angles defined by the Cp* centroids (Cp*$_{cent}$), Rh centers, and centroids calculated between the phosphorus atoms to be compressed in **2** (149.2°/148.5°) relative to **1** (153.9°), no doubt an influence of the constrained geometry of ligand binding. The Rh–Cl distances of 2.383(2) Å for **1** and 2.395(1) Å/2.398(1) Å for **2** are similar, consistent with the common formal +III oxidation state of rhodium for both complexes.

To our delight, both **1** and **2** could be reduced to the corresponding formally Rh(I) complexes **3** and **4**, respectively, upon treatment with sodium amalgam in THF (see Scheme 1). Consistent with prior results using the dppb ligand, the solution darkens over the course of the reaction. Extraction of the crude material with hexane afforded **3** and **4** in pure form as light brown and dark brown solids, respectively. Characterization of the desired, pure forms of **3** and **4** by ^{1}H NMR reveals similar Cp* triplets in each

case, now shifted downfield to 2.12 and 1.36 ppm, respectively, attributable to the increased electron density about the rhodium metal center upon reduction (all NMR data for **3** and **4** can be found in the SI, Figures S11–S18). The coupling constants between the equivalent Cp* methyl protons and the phosphorus atoms decrease for the Rh(I) complexes in comparison with the Rh(III) forms ($^4J_{H,P}$ = 2.4 Hz for **3**; $^4J_{H,P}$ = 1.7 Hz for **4**), a feature attributable again to the increased electron density about rhodium. The $^{31}P\{^1H\}$ NMR spectra for **3** and **4** give only the expected doublets corresponding to the bound diphosphine ligands (δ = –12.28 ppm, $^1J_{P,Rh}$ = 190.2 Hz for **3**; δ = 51.46 ppm, $^1J_{P,Rh}$ = 227.2 Hz for **4**). As observed previously in our dppb complexes, the value of $^1J_{P,Rh}$ increases significantly upon reduction, consistent with increased back donation from the electron-rich metal center.

Due to the change of geometry about the rhodium metal center upon reduction (*vide infra*), the formerly diastereotopic methylene protons in **1** become homotopic in **3**, as demonstrated by the single resonance integrating to 2H at 3.80 ppm (td, $^2J_{H,P}$ = 10.5 Hz, $^3J_{H,Rh}$ = 1.4 Hz). Notably, the geminal methyl groups of **4** are also equivalent, corresponding to a lone singlet integrating to 6H at 1.65 ppm. This result contrasts with the crystallographic data (see Figure 1), implying that the complex behaves more symmetrically (apparent *pseudo*-C_{2v} geometry) in solution that differs from the solid-state structure (*pseudo*-C_s). Fluxionality in the Xantphos backbone may contribute to these observations, such that the form of the complex in solution relaxes the θ values closer to 180°, resembling the solid-state form of **3** (see Table 1). The T-shaped geometry imparted by such a relaxation would render the two methyl groups on the Xantphos backbone equivalent and, thereby, homotopic, as they appear in the ^1H NMR spectral data.

Table 1. Bond Lengths (Å) and Angles (°) of Compounds **1**–**6**.

	Rh–P length	Rh–Cp*$_{cent}$ length	∠P–Rh–P	θ (∠Cp*$_{cent}$–Rh–P1/P2$_{cent}$)
1	2.325(1), 2.311(1)	1.846	72.20(5)	153.9
2	2.383(1), 2.378(1); 2.376(1), 2.369(4)	1.888; 1.882	95.38(3); 95.69(3)	149.2; 148.5
3	2.192(1), 2.211(1)	1.925	73.04(2)	179.3
4	2.231(1), 2.237(1)	1.983	96.96(3)	164.7
5	2.258(1)	1.878	73.20(3)	158.2
6	2.297(1), 2.305(1); 2.296(1), 2.305(1)	1.925; 1.928	97.56(3); 98.35(3)	154.1; 152.9

Single crystals of **3** and **4** suitable for XRD analysis were obtained by slow cooling of concentrated solutions of **3** in hexane and of **4** in hexane containing 2 drops of toluene. The solid-state structures (see Figure 1) show the geometries about the formally Rh(I) centers to be distorted T-shapes in both cases. Each rhodium center has a first coordination sphere containing the [η^5-Cp*] ligand and the expected κ^2-diphosphine ligand (see Table 1). In **3**, the T-shape is quite tight, with a value for θ of 179.3°, near the ideal value of 180° and similar to the value of 177.3° found for Cp*Rh(bpy).[19] On the other hand, the θ value of 164.7° for **4** reveals greater distortion, again attributable to the non-planar nature of the eight-membered rhodacycle induced by the rather rigid structure of the Xantphos backbone. As expected, the P–Rh–P angles do not change significantly (< 1°) in either system upon reduction, confirming the limited flexibilities of dppm and Xantphos in this regard. And, as observed with our dppb system, reduction results in significant elongation of the Rh–Cp*$_{cent}$ distances, consistent with the π-donating nature of Cp*, the electron-rich character of rhodium(I), and the anticipated greater ionic radius for Rh(I) vs. Rh(III).[20] Taken together, these findings support the versatility and modularity of [Cp*Rh] diphosphine chemistry across multiple oxidation states.

Upon successful isolation of both Rh(I) complexes, we were able to prepare the corresponding rhodium hydride species. Reacting 1 equivalent of **3** or **4** with 0.95 equivalents of anilinium triflate (pK_a = 10.6 in MeCN[14]) in 1:1 MeCN/THF furnished the desired monomeric rhodium hydrides **5** and **6**, respectively. The slightly substoichiometric amount of acid was utilized for the purpose of simplifying purification of the products; having even slight unreacted acid present during workup resulted in compromised purity during fractionation due to its similar solubility with the hydride. Characterization of both **5** and **6** by ^1H NMR showed characteristic resonances corresponding to the hydride ligand bound to rhodium at –9.74 ppm (q, $^1J_{H,Rh}$ = 27.4 Hz, $^2J_{H,P}$ = 27.4 Hz) and –11.04 ppm (td, $^2J_{H,P}$ = 33.7 Hz, $^1J_{H,Rh}$ = 17.7 Hz), respectively (all NMR data for **5** and **6** can be found in the SI, Figures S19–S31). Additionally, the Cp* signal appears in both spectra as a triplet of doublets (δ = 1.81 ppm, $^4J_{H,P}$ = 3.5 Hz, $^4J_{H,H}$ = 1.2 Hz for **5**; δ = 1.11 ppm, $^4J_{H,P}$ = 3.4 Hz, $^4J_{H,H}$ = 1.2 Hz for **6**), indicating that the hydride couples to the 15 equivalent methyl protons of the Cp* ligand.

The methylene protons of **5** are diastereotopic, as they were in **1**. These protons appear as two separate but complex groupings of resonances (each centered near 4.86 and 3.98 ppm), integrating to 1H each for the expected total of two methylene protons. The more downfield signal, which appeared as a dtd in **1**, is additionally split by the hydride ligand in **5** to give rise to a dtdd (δ = 4.86 ppm; $^2J_{H,H}$ = 16.2 Hz, $^2J_{H,P}$ = 9.7 Hz, $^3J_{H,Rh}$ = 4.5 Hz, $^4J_{H,H}$ = 3.2 Hz),[21] while the further upfield methylene proton remains a dt that is shifted upfield relative to **1** (δ = 3.98 ppm; $^2J_{H,H}$ = 16.2 Hz, $^2J_{H,P}$ = 12.1 Hz). These complex splitting patterns were assigned with the aid of multifrequency NMR studies and can be successfully and faithfully reproduced with digital simulations incorporating both first- and second-order field effects (*vide infra*). The diastereotopic geminal methyl groups of **6** also appear as two distinct singlets, as was the case in **2**.

The $^{31}P\{^1H\}$ NMR spectrum for **5** includes the expected doublet for the dppm ligand (δ = 1.34 ppm, $^1J_{P,Rh}$ = 119.2 Hz). However, the spectrum for **6** shows a dd (δ = 41.32 ppm, $^1J_{P,Rh}$ = 148.2 Hz, $^2J_{P,H}$ = 6.3 Hz), indicating a small but observable coupling between the phosphorus atoms of Xantphos and the hydride ligand, despite the proton decoupling for this spectrum. This finding is attributable to the finite bandwidth of the 2.8 kHz WALTZ-16 ^1H-decoupling[22] in the standard $^{31}P\{^1H\}$ experiment acquired on our 400 MHz NMR spectrometer. ^1H decoupling[23] does not follow a strict turn-on/turn-off behavior, but rather a non-linear, sine-like chemical shift dependence with incomplete decoupling (sometimes referred to as "spin tickling") of ^1H resonances outside of the nominal range of –3 to 11 ppm, as determined by our experimental parameters.[24] The observation of complete decoupling for **5** and

only partial decoupling for **6** is attributable to the influence of decoupling sidebands at the respective resonance frequencies for these compounds.[25]

Vapor diffusion of diethyl ether into concentrated THF solutions of **5** and **6** afforded crystals suitable for XRD analysis in both cases. The solid-state structures (see Figure 1) confirm the geometries about the formally Rh(III) centers to be *pseudo*-octahedral, as they were in **1** and **2**. The geometry of each rhodium center has changed significantly from the cases of **3** and **4**, as judged by the θ values (158.2° and 154.1°/152.9° for **5** and **6**, respectively), confirming distortion away from the T-shaped geometries found for the Rh(I) compounds (see Table 1). Gratifyingly, the hydride ligands (labeled as H1 for **5** and **6** in Figure 1) were both located in Fourier difference maps, and their positions were freely refined in the final XRD data modeling. Infrared spectroscopic data confirm the Rh–H stretching frequencies for these new compounds in the expected region, with values of 1982 and 1936 cm^{-1}, respectively, for **5** and **6** (see SI, Figures S32–S33). These values compare well with the corresponding value measured for **B** of 1986 cm^{-1}.[13] In light of all these data, the sequential reduction/protonation route can be concluded to be effectively modular for preparation of [Cp*Rh] monohydride complexes supported by diphosphine ligands, complementing existing examples from the literature.

Chemical Properties of the Rh–H Species. With full characterization in hand, we next examined the chemical and spectral properties of the two new [Cp*Rh] hydride species. A comparison of the hydride resonances in the ^{1}H NMR spectra of **B**, **5**, and **6** provides insight into the effect of rhodacycle size on the splitting of the hydride resonance. The rhodacycles in **5**, **B**, and **6** are 4-, 5-, and 8-membered, respectively; as seen in Figure 2, these different sizes give rise to different splitting patterns and chemical shifts for each hydride resonance. Most notably, the splitting pattern of each broadened hydride resonance can be seen trending from a quartet to a triplet of doublets as the rhodacycle size increases, due to both increased coupling between the hydride and the pendant phosphorus atoms ($^2J_{H,P}$ = 27.4 Hz, 29.1 Hz, and 33.7 Hz for **5**, **B**, and **6**, respectively) and decreased coupling between the hydride and rhodium ($^1J_{H,Rh}$ = 27.4 Hz, 25.4 Hz, and 17.7 Hz for **5**, **B**, and **6**, respectively) as the rhodacycle size increases.

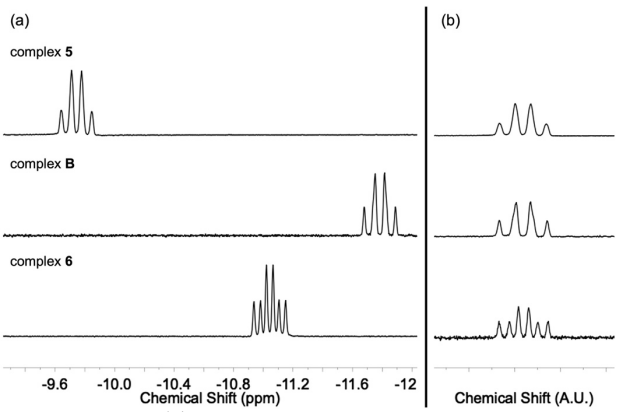

Figure 2. Panel (a): Stacked ^{1}H NMR spectra depicting the hydride ligand resonance of the formally Rh(III) hydride complexes **5**, **B**, and **6**. Panel (b): Stacked ^{1}H NMR spectra depicting the hydride resonances of **5**, **B**, and **6** aligned vertically (with arbitrary units on the x-axis).

We next sought to investigate the hydrogen evolution capabilities of **5** and **6**. Prior work has demonstrated that [Cp*Rh] hydride species have unique hydrogen evolution properties depending on the bidentate ligand chosen for the given scaffold. Work with bpy-ligated [Cp*Rh] complexes has shown that treatment of the formally Rh(I) species with anilinium triflate (pK_a = 10.6 in MeCN[14]) gives rise to the Cp*H form of the complex, which is sufficiently basic to produce hydrogen upon addition of another equivalent of the same acid.[5b] Work with the mixed-ligand PQN system showed that the Rh–H, formed upon protonation of the Rh(I) species by anilinium triflate (**H**, Chart 1), was isolable and characterizable; however, the only acid with which this hydride was able to evolve hydrogen was $[DMFH]^+[OTf]^-$ (pK_a = 6.1 in MeCN[26]).[12] Finally, the dppb-ligated Rh–H species (**B**) was not sufficiently basic to evolve hydrogen in the presence of either of these acids, even after heating to 50 °C in the presence of $[DMFH]^+[OTf]^-$.[13]

In order to probe the reactivity of these new hydride species, we subjected **5** and **6** to $[DMFH]^+[OTf]^-$ in CD_3CN (see SI, pp. S19–S20 for experimental details and ^{1}H NMR spectra). Both hydride complexes were stable at room temperature in the presence of this acid for up to 6 days. Heating each of these samples to 65 °C for an additional 48 hours showed the formation of small triplets near the td of the Cp* methyl protons in the ^{1}H NMR spectrum of each compound, attributable to new Cp*-bound species, likely solvento Rh(III) complexes formed upon evolution of hydrogen (see SI, p. S19). Dihydrogen was not observed in the NMR spectra, however, consistent with a very low yield and/or loss from the J. Young tubes; the new Cp* species correspond to conversion of less than 3 % of the starting hydride material in both instances. These findings underscore the high stability of Rh–H complexes supported by diphosphine ligands relative to previously studied diimine ligand systems, even in the presence of a strong acid.

Multifrequency NMR Characterization of 1 and 5. As described above, compounds **1**-**6** display rich NMR spectroscopic properties due to the presence of multiple spin-active nuclei in each system, including H, C, P, and Rh. Particularly for **1** and **5**, the spectra of these compounds are among the most complex that we have encountered in our work with organometallic rhodium systems, a situation arising from the presence of the diastereotopic methylene protons in the backbone of the dppm ligand. The diastereotopic nature of these protons, evidenced by so-called "roofing" behavior of their corresponding resonances, is diagnostic of the *pseudo*-octahedral geometry of the rhodium centers in **1** and **5**. Second-order effects such as roofing are not often difficult to interpret, but the additional involvement here of multiple heteronuclear couplings gives rise to the intricately split resonances, highlighting the complexity of the chemical and magnetic environments of these geminal protons and muddling simple interpretations. Therefore, we pursued multifrequency experiments to elucidate the magnetic and chemical nature of these protons.

Multifrequency NMR experiments provide the opportunity to resolve the second-order field effects that give rise to the roofing phenomenon which we observed for the diastereotopic methylene protons of **1** and **5**. Increasing the B_0 field (i.e., ^{1}H resonant frequency) diminishes the deviation from typical first-order behavior caused by such effects, and thus can simplify spectral interpretation (see Figure 3).[27] Second-order effects arise when the coupling constant between chemically and magnetically inequivalent nuclei are on the same order of magnitude as the difference between their

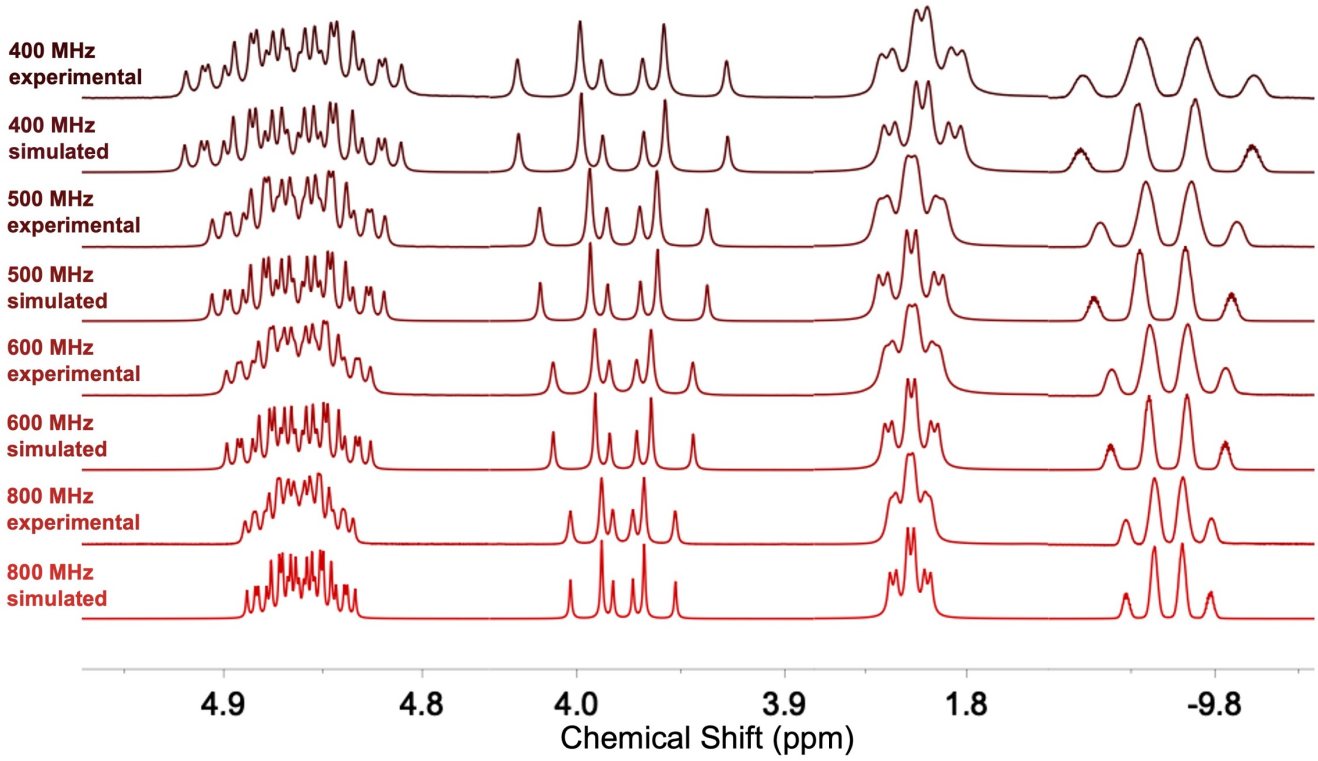

Figure 3. Stacked, partial multifrequency ^{1}H NMR spectra of **5**, depicting alternating experimental and simulated spectra for both methylene protons, the Cp* methyl protons, and the hydride ligand (from left to right). Resonances are not shown to scale.

chemical shifts (e.g., $J \approx \Delta\delta$). As $\Delta\delta$ (in units of Hz rather than the more commonly encountered units of ppm) is a quantitative measure of magnetic inequivalence, increasing the magnetic field strength of the spectrometer (which increases the value of $\Delta\delta$ in Hz) can minimize the appearance of second-order effects by moving toward a situation where $J << \Delta\delta$. In general, at a high-field limit (which may or may not be accessible for a given system based on the exact values of J and $\Delta\delta$), a spectrum may be made to appear first-order.[28] Based on the appearance of the resonances corresponding to the methylene protons of dppm within **1** and **5** (corresponding to H35A/H35B and H19A/H19B, respectively, that were identified in the crystallography; see Figure 1), we anticipated that the observable second-order effects could be minimized as the field frequency was increased.

Indeed, the ^{1}H NMR spectra of **1** collected at 400, 500, 600, and 800 MHz show decreased roofing between the methylene protons as the frequency of the instrument increases (see SI, Figure S36). The roofing is still visible at 800 MHz, which can be explained if we consider the ratio of the difference between the chemical shifts ($\Delta\delta$ in Hz) and the relevant coupling constant ($^{2}J_{H,H}$ in Hz); the larger this quotient, the less observable the second-order field effects will be in a given spectrum (for H35A/H35B: at 400 MHz, 163.3 Hz/15.6 Hz = 10.5; at 800 MHz, 320.7 Hz/15.7 Hz = 20.4). A larger $\Delta\delta$ (in Hz, at a given field frequency) gives a larger ratio when divided by the coupling constant, confirming that the second-order field effects are minimized when $\Delta\delta$ is larger. Relative to **1**, the effects of increasing the field strength on the methylene protons were far more noticeable for **5** due to the greater difference in chemical shift ($\Delta\delta$ value) for H19A/H19B in **5** vs. the corresponding protons in **1**. For H35A/H35B in **1**, the $\Delta\delta$ is much smaller than that of H19A/H19B in **5** ($\Delta\delta$ = 0.40 ppm for **1**, 0.88 ppm for **5**). Indeed, the roofing observed for H19A/H19B in **5** at 400 MHz is essentially eliminated in the spectrum obtained at 800 MHz (see SI, Figure S37), an occurrence not reached for H35A/H35B in **1**, as the roofing was still clearly observable for those methylene protons even at 800 MHz. Taken together, these parameters quantify the effect of the inequivalence of the methylene protons on the spectral data in both systems and set the stage for a full assignment of the coupling networks underlying their appearance in the data.

Digital NMR Simulations for 1 and 5. In order to assign the coupling networks involving the methylene protons in complexes **1** and **5**, as well as confirm the field-dependence of the observed experimental data, spectral simulations of the NMR data for **1** and **5** were performed using the Spin Simulation function of the MestReNova software package.[29] Full details regarding these simulations can be found in the SI (pp. S22–S23). Generally speaking, simulations serve as a powerful tool to aid in understanding the coupling interactions between NMR-active nuclei because individual couplings in a given network can be activated or deactivated on-demand during spectral visualization, affording insights from pattern recognition that would not be available otherwise. For **1**, the spin system can be described as $ABM_{15}Y_2Z$ in Pople notation,[30] where A and B are methylene protons H35A/H35B, M_{15} refers to the Cp* methyl protons, Y_2 represents the two phosphorus atoms of dppm, and Z represents the rhodium metal center.[31] In accord with this spin system assignment, the expected dtd and dt resonances for each methylene proton were reproduced to a very high degree across all frequencies by the simulations (see SI, Figure S38).

With this understanding of the spin system of **1** in hand, we turned our attention to the more complex system present in **5**. For these simulations, we expanded the simulation spectral window to

model both resonances arising due to the hydride ligand as well as the Cp* methyl resonances (for reasons discussed below, *vide infra*). This system can be described as $ABM_{15}XY_2Z$, similar to that of **1**, but with substitution of the protons corresponding to H19A/H19B as A and B and inclusion of the hydride ligand as X.[31] Appealingly, the simulated spectrum closely models the experimental spectrum of **5** at 400 MHz (see Figure 3, uppermost two spectra).

The observable broadening of the quartet resonance for the hydride ligand (Figure 3, rightmost side of the spectra) is the direct result of coupling to the 15 Cp* methyl protons at 1.2 Hz; such coupling of the hydride to the many equivalent Cp* methyl protons at a low magnitude gives rise to the broadened shape. To confirm this situation, the individual couplings involving the hydride were investigated with sequential simulations of increasing complexity to probe the consequences in the final appearance of the hydride resonances (see SI, Figure S39). The simulations support this hypothesis regarding the origin of the broadening of the hydride resonances, in that the quartet for the hydride of **5** could be simulated when only coupling of the hydride to rhodium and phosphorus is considered (see SI, Figure S39, spectrum 5). Additionally, the quartet of doublets expected from coupling of the hydride in **5** to only rhodium, phosphorus, and one methylene proton is also confirmed through the simulation (see SI, Figure S39, spectrum 4). The splitting of the dtdd methylene proton and the td Cp* methyl proton resonances correspondingly deviate from the appearance of the experimental data when coupling to the hydride is omitted, further supporting their role in the broadness of the quartet of the hydride (see SI, Figure S39 for the total collection of these simulations and details on each of them).

Taken together, the multifrequency experimental studies and paired comprehensive simulations of **1** and **5** help disentangle the chemical and magnetic complexity of these systems and resolve the nature of the inequivalence of several of the nuclei in these systems. The second-order field effects giving rise to the appearance of roofing about the methylene protons can be understood and are nearly resolved by moving to spectrometers that operate at higher frequencies; at 800 MHz, the second-order effects remain visible, however, due to the intrinsic value of $\Delta\delta$ for the methylene protons. Nonetheless, the simulations of **1** and **5** faithfully reproduce the needed resonances and splitting patterns in all cases, providing a concrete inventory of the nuclear coupling interactions that govern the spectral properties of both **1** and **5**.

Absolute Assignment of Methylene Protons in 5. The chemical inequivalence of the methylene protons present in the dppm backbone of **5** encouraged us to pursue an absolute assignment of the spectral signatures associated with these individual H-atoms. These are labelled as H19A and H19B in the related solid-state structure obtained from single-crystal XRD analysis (see Figure 4). To accomplish the spectral assignment, 2D-NMR experiments were conducted (see SI, Figures S29–S31). NOESY NMR data indicate that the more downfield methylene resonance (δ = 4.89 ppm, dtdd) is spatially close to the aromatic protons observed at 7.36 ppm in a way that the dt at 3.98 ppm is not; these aromatic protons appear as a dtd and correspond to four of the protons on the phenyl rings of the dppm ligand. In turn, these four aromatic protons are spatially close to the Cp* methyl protons according to NOESY, a finding which points to their proximity to the Cp* ring. Of the four phenyl rings of the dppm ligand (see Figure 4), the two rings shown as oriented up and to the left in the solid-state structure are in closer proximity to the Cp* ring; as a result, the 4H dtd at 7.36 ppm most likely belongs to the four *ortho* protons of those two phenyl rings. On the basis of this coupling map, we assign the dtdd at 4.89 ppm as corresponding to the diastereotopic methylene proton which is oriented upward toward the Cp* ring in **5**. This corresponds to H19B in the XRD data. By elimination, the downward-facing proton (labeled as H19A in the XRD data) can thus be assigned as the dt at 3.98 ppm. This assignment is supported by the XRD data, in that strong NOESY cross-peaks occur when the distance between two atoms is near 2.5 Å, with medium and weak cross-peaks occurring at distances near 3.5 Å and 5.0 Å, respectively.[32] The closer proximity of H19B to the nearest *ortho* proton in the solid-state structure (2.58 Å) relative to H19A (3.97 Å) is in harmony with the stronger cross-peak present in the NOESY spectral data for the dtdd. Therefore, we can confidently identify H19A as the dt at 3.98 ppm and H19B as the dtdd at 4.89 ppm in the ^{1}H NMR data for **5**.

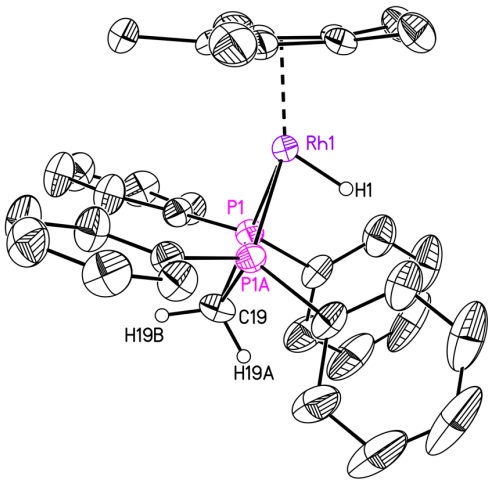

Figure 4. Solid-state structure of the dppm-supported monohydride **5** showing terminal phenyl rings. Displacement ellipsoids are shown at 50% probability level. Hydrogen atoms (except H19A, H19B, and H1) and triflate counteranion are omitted for clarity.

CONCLUSIONS

This work demonstrates the synthetic modularity of our sequential reduction/protonation route in the context of preparation, isolation, and characterization of two new [Cp*Rh] monohydride complexes bearing the diphosphine ligands dppm and Xantphos. The synthesis of these compounds is remarkably straightforward, considering the relative scarcity of such compounds in the literature, and enables preparation of both Rh(III) and Rh(I) complexes through redox transformations. All structures were characterized by NMR methods as well as single-crystal X-ray diffraction analysis, and the hydrides were additionally characterized by IR spectroscopy. The complexities of the nuclear spin systems featured in the Rh(III) dppm compounds were elucidated using both multifrequency experimental studies and comprehensive digital simulations. The findings explain the inequivalence of the diastereotopic methylene protons and enable faithful replication of the diagnostic experimental data through reliable coupling constant assignments obtained with digital NMR simulations. The

simulations clarified the spin systems which give rise to the complex splitting patterns displayed by **5,** in particular, demonstrating that the hydride ligand couples to rhodium, both phosphorus atoms, the Cp* methyl protons, and one of the methylene protons. These assignments would have been tentative at best if not for the use of simulations, as the coupling of the hydride to both the Cp* methyl protons and one methylene proton could not be measured directly from the broadened quartet corresponding to the hydride. The absolute assignment of both methylene protons, aided by 2D NMR experiments, allowed us to relate the geometry observed in the crystal structure to the spectroscopic data. Taken together, these results demonstrate the power of the reduction/protonation synthetic sequence, and the efficacy of multifrequency NMR to characterize new and challenging reaction products.

EXPERIMENTAL SECTION

General Considerations

All manipulations were carried out in dry N_2-filled gloveboxes (Vacuum Atmospheres Co., Hawthorne, CA, USA) or under an N_2 atmosphere using standard Schlenk techniques, unless otherwise noted. All solvents were of commercial grade and dried over activated alumina using a PPT Glass Contour (Nashua, NH, USA) solvent purification system prior to use, and were stored over molecular sieves. All chemicals were obtained from major commercial suppliers and used as received after extensive drying. $[Cp^*RhCl_2]_2$ was prepared according to literature methods with minor modifications.[4]

Deuterated solvents for NMR studies were purchased from Cambridge Isotope Laboratories (Tewksbury, MA, USA); CD_3CN was dried with CaH_2 and stored over molecular sieves, and C_6D_6 was dried over sodium/benzophenone. ^1H, ^{13}C, ^{19}F, and ^{31}P NMR spectra were collected with 400, 500, 600, or 800 MHz Bruker spectrometers and were referenced to the residual protio-solvent signal in the cases of ^1H and ^{13}C unless otherwise noted.[33] Heteronuclear NMR spectra were referenced to the appropriate external standard following the recommended scale based on ratios of absolute frequencies (Ξ). ^{19}F NMR spectra are reported relative to CCl_3F, and ^{31}P NMR spectra are reported relative to H_3PO_4.[34,35] Chemical shifts (δ) and coupling constants (*J*) are reported in ppm and Hz, respectively. Simulations of NMR spectra were carried out using the Advanced Spin Simulation program in MestReNova (Mestrelab Research, chemistry software solutions). IR spectra were collected using a Shimadzu IRSpirit Fourier Transform Infrared Spectrometer in transmission mode using a high-throughput diamond QATR-S single reflection attenuated total reflectance attachment at an incident angle of 45 degrees. Elemental analyses were performed by Midwest Microlab, Inc. (Indianapolis, IN). Elemental analysis could not be obtained for **3**, **4**, **5**, or **6** due to their acute air sensitivity, but was obtained for **2**. Analysis for **1** has been reported previously.[18]

Synthetic Procedures.

Synthesis of $[Cp^*Rh(dppm)Cl]PF_6$ (**1**): To a 20-mL scintillation vial equipped with a Teflon stir bar, $[Cp^*RhCl_2]_2$ (0.062 g, 0.100 mmol) was dissolved in MeCN (ca. 2 mL) to give a red suspension. To this suspension, $AgPF_6$ (0.051 g, 0.20 mmol) in MeCN (ca. 2 mL) was added, and the solution immediately changed from red to orange upon formation of AgCl as a white precipitate. The solution was allowed to stir for 5 min, then the resulting AgCl precipitate was filtered off over Celite into a 25-mL Schlenk flask. To this solution were added a Teflon stir bar and dppm (0.119 g, 0.20 mmol) dissolved in THF (ca. 2 mL). The Schlenk flask was closed and capped with a greased glass stopper, removed from the glovebox, connected to the Schlenk line, and stirred overnight at 65 °C under N_2. The next day, the flask was opened to air and the orange solution was concentrated. The resulting material was transferred to a 500-mL Erlenmeyer flask with minimal MeCN and a large excess of diethyl ether (ca. 300 mL) was added, causing precipitation of the desired product in the freezer overnight. The yellow solid was then filtered and washed thoroughly with diethyl ether to afford the title compound. Yield: 0.143 g (89 %). ^1H NMR (400 MHz, CD_3CN): δ = 7.65 – 7.51 (m, 12H), 7.48 (td, 4H, *J* = 7.6, 7.1, 3.8 Hz), 7.30 – 7.22 (m, 4H), 4.91 (dtd, 1H, *J* = 15.6, 10.1, 1.7 Hz), 4.51 (dt, 1H, *J* = 15.6, 13.0 Hz), 1.74 (t, 15H, *J* = 4.1 Hz) ppm. $^{13}C\{^1H\}$ NMR (126 MHz, CD_3CN): δ = 133.61 (td, *J* = 5.7, 4.0 Hz), 133.33 (d, *J* = 1.8 Hz), 132.80 (d, *J* = 1.5 Hz), 130.39 – 130.21 (m), 130.05 – 129.82 (m), 104.77 (dt, *J* = 6.1, 3.2 Hz), 40.32 (d, *J* = 28.5 Hz), 10.21 ppm. ^{19}F NMR (376 MHz, CD_3CN): δ = –73.81 (d, *J* = 706.2 Hz) ppm. $^{31}P\{^1H\}$ NMR (162 MHz, CD_3CN): δ = –6.26 (d, $^1J_{P,Rh}$ = 115.1 Hz), –145.48 (septet) ppm.

Synthesis of $[Cp^*Rh(Xantphos)Cl]PF_6$ (**2**): To a 20-mL scintillation vial equipped with a Teflon stir bar, $[Cp^*RhCl_2]_2$ (0.062 g, 0.100 mmol) was dissolved in MeCN (ca. 2 mL) to give a red suspension. To this suspension, $AgPF_6$ (0.051 g, 0.20 mmol) in MeCN (ca. 2 mL) was added, and the solution immediately changed from red to orange upon formation of AgCl as a white precipitate. The solution was allowed to stir for 5 min, then the resulting AgCl precipitate was filtered off over Celite into a 25-mL Schlenk flask. To this solution were added a stirbar and Xantphos (0.119 g, 0.21 mmol) dissolved in THF (ca. 2 mL). The Schlenk flask was closed and capped with a greased glass stopper, removed from the glovebox, connected to the Schlenk line, and stirred overnight at room temperature. The next day, the flask was opened to air and the resulting bright red solution was concentrated. The resulting material was transferred to a 500-mL Erlenmeyer flask with minimal MeCN and a large excess of diethyl ether (ca. 300 mL) was added, causing precipitation of the desired product in the freezer overnight. The orange solid was then filtered and washed thoroughly with diethyl ether to afford the title compound. Yield: 0.168 g (84 %). ^1H NMR (400 MHz, CD_3CN): δ = 7.87 (dd, 2H, *J* = 7.6, 1.6 Hz), 7.77 – 7.68 (m, 4H), 7.63 – 7.39 (m, 10H), 7.05 (s, 4H), 6.90 (tt, 2H, *J* = 7.4, 1.1 Hz), 6.70 (t, 4H, *J* = 7.7 Hz), 2.00 (s, 3H), 1.68 (s, 3H), 0.97 (t, 15H, *J* = 4.1 Hz) ppm. $^{13}C\{^1H\}$ NMR (126 MHz, CD_3CN): δ = 155.38 (t, *J* = 3.0 Hz), 137.31 (t, *J* = 5.7 Hz), 136.50 – 136.29 (m), 132.70, 131.95, 130.84 (t, *J* = 1.9 Hz), 130.06, 129.59 – 129.34 (m), 129.31 – 128.97 (m), 125.94 (t, *J* = 3.9 Hz), 106.27 (ddd, *J* = 8.7, 5.9, 2.2 Hz), 37.72, 31.29, 22.73, 9.48 ppm. ^{19}F NMR (376 MHz, CD_3CN): δ = –73.80 (d, *J* = 706.3 Hz) ppm. $^{31}P\{^1H\}$ NMR (162 MHz, CD_3CN): δ = 18.29 (d, $^1J_{P,Rh}$ = 143.4 Hz), –144.63 (septet) ppm. Anal. Calcd. for $C_{49}H_{47}ClF_6OP_3Rh$: C, 59.02; H, 4.75. Found: C, 59.06; H, 4.82.

Synthesis of Cp*Rh(dppm) (**3**): A suspension of **1** (0.033 g, 0.04 mmol) in THF (ca. 2 mL) was added to a 20-mL scintillation vial containing 1% Na(Hg) (0.020 g, 0.89 mmol Na, ca. 20 equiv.). The yellow suspension darkened immediately to a dark orange color and continued to darken while stirring overnight. The next day, the reaction solution was filtered through Celite to remove Hg and $NaPF_6$ precipitate. THF was then removed in vacuo and the resulting solid was extracted with hexanes to obtain the title compound as a light brown solid. Yield: 0.024 g (92 %). ^1H NMR (400 MHz, C_6D_6): δ = 7.69 (dddd, 8H, *J* = 8.1, 6.9, 5.7, 1.4 Hz), 7.12 (tt, 8H, *J* = 7.0, 0.9 Hz), 7.08 – 7.01 (m, 4H), 3.80 (td, 2H, *J* = 10.5, 1.4 Hz), 2.12 (t, 15H, *J* = 2.4 Hz) ppm. $^{13}C\{^1H\}$ NMR (126 MHz, C_6D_6): δ = 140.18 – 139.50 (m), 132.60 – 132.06 (m), 128.81, 94.24 (q, *J* = 3.6 Hz), 52.07 – 51.00 (m), 11.99 ppm. $^{31}P\{^1H\}$ NMR (162 MHz, C_6D_6): δ = –12.28 (d, $^1J_{P,Rh}$ = 190.2 Hz) ppm.

Synthesis of Cp*Rh(Xantphos) (**4**): A suspension of **2** (0.051 g, 0.05 mmol) in THF (ca. 2 mL) was added to a 20 mL scintillation vial containing freshly prepared 1% Na(Hg) (0.023 g, 1.0 mmol Na, ca. 20 equiv.). The orange suspension darkened immediately to a deep

brown color and continued to darken while stirring overnight. The next day, the reaction solution was filtered through Celite to remove Hg and $NaPF_6$ precipitate. THF was then removed in vacuo and the resulting solid was extracted with hexanes to obtain the title compound as a dark brown solid. Yield: 0.037 g (88 %). ^{1}H NMR (400 MHz, C_6D_6): δ = 7.63 (s, 8H), 7.39 – 7.32 (m, 2H), 7.19 (dd, 2H, *J* = 7.7, 1.2 Hz), 6.88 (t, 2H, *J* = 7.6 Hz), 6.81 (s, 12H), 1.65 (s, 6H), 1.36 (t, 15H, *J* = 1.7 Hz) ppm. ^{13}C{^{1}H} NMR (126 MHz, C_6D_6): δ = 156.11 (t, *J* = 4.0 Hz), 139.05, 135.92, 99.10 – 96.73 (m), 36.91, 29.88, 10.77 ppm. ^{31}P{^{1}H} NMR (162 MHz, C_6D_6): δ = 51.46 (d, $^1J_{P,Rh}$ = 227.2 Hz) ppm.

Synthesis of [Cp*Rh(dppm)H]OTf (**5**): To a red suspension of **3** (0.021 g, 0.033 mmol) in the minimum amount of 1:1 THF/MeCN (ca. 2 mL) was added a solution of anilinium triflate (0.008 g, 0.031 mmol) in MeCN (ca. 1 mL). The solution immediately became yellow in color. The vial was capped, and the solution was allowed to stir for 1 hr. The solvent was then removed in vacuo and the solid was fractionated with hexane, diethyl ether, toluene, and THF to obtain the title compound from THF as a light yellow solid. Yield: 0.023 g (89 %). ^{1}H NMR (400 MHz, CD_3CN): δ = 7.64 – 7.48 (m, 16H), 7.36 (dtd, 4H, *J* = 8.5, 6.6, 1.3 Hz), 4.86 (dtdd, 1H, *J* = 16.2, 9.7, 4.5, 3.2 Hz), 3.98 (dt, 1H, *J* = 16.2, 12.1 Hz), 1.81 (td, 15H, *J* = 3.5, 1.2 Hz), –9.74 (q, 1H, *J* = 27.4 Hz) ppm. ^{13}C{^{1}H} NMR (126 MHz, CD_3CN): δ = 133.59 (t, *J* = 6.8 Hz), 132.89, 132.84 – 132.68 (m), 132.50, 130.03 (dt, *J* = 16.5, 5.9 Hz), 102.22 (q, *J* = 3.1 Hz), 47.32 – 46.65 (m), 21.38, 10.52 ppm. ^{19}F NMR (376 MHz, CD_3CN): δ = –80.16 ppm. ^{31}P{^{1}H} NMR (162 MHz, CD_3CN): δ = 1.34 (d, $^1J_{P,Rh}$ = 119.2 Hz) ppm. IR Spectroscopy: ν (cm^{-1}) = 1982 (Rh–H).

Synthesis of [Cp*Rh(Xantphos)H]OTf (**6**): To a brown suspension of **4** (0.033 g, 0.040 mmol) in the minimum amount of 1:1 THF/MeCN (ca. 2 mL) was added a solution of anilinium triflate (0.009 g, 0.037 mmol) in MeCN (ca. 1 mL). The solution immediately became dark yellow in color. The vial was capped and the solution was allowed to stir for 1 hr. The solvent was then removed in vacuo and the solid was fractionated with hexane, diethyl ether, toluene, and THF to obtain the title compound from THF as a yellow solid. Yield: 0.029 g (80 %). ^{1}H NMR (400 MHz, CD_3CN): δ = 7.84 (dd, 2H, *J* = 7.8, 1.3 Hz), 7.76 (tdd, 4H, *J* = 8.0, 3.8, 1.9 Hz), 7.60 (ddd, 2H, *J* = 7.6, 5.3, 2.1 Hz), 7.51 (tdd, 6H, *J* = 7.4, 4.5, 1.9 Hz), 7.46 – 7.40 (m, 2H), 6.87 – 6.62 (m, 10H), 2.01 (s, 3H), 1.70 (s, 3H), 1.11 (td, 15H, *J* = 3.4, 1.2 Hz), –11.04 (td, 1H, *J* = 33.7, 17.7 Hz) ppm. ^{13}C{^{1}H} NMR (126 MHz, CD_3CN): δ = 155.87 (d, *J* = 3.4 Hz), 137.05, 136.73 – 136.04 (m), 132.28, 130.37 (d, *J* = 13.9 Hz), 129.50 (t, *J* = 5.7 Hz), 129.30, 125.43 – 124.97 (m), 104.59 (d, *J* = 5.3 Hz), 37.89, 30.99, 22.78, 10.11 ppm. ^{19}F NMR (376 MHz, CD_3CN): δ = –80.19 ppm. ^{31}P{^{1}H} NMR (162 MHz, CD_3CN): δ = 41.32 (dd, $^1J_{P,Rh}$ = 148.2, $^2J_{P,H}$ = 6.3 Hz) ppm. IR Spectroscopy: ν (cm^{-1}) = 1936 (Rh–H).

X-ray Crystallography

Single crystals of **1** were obtained by vapor diffusion of diethyl ether into a concentrated acetonitrile solution of the complex. Single crystals of **2** were obtained by vapor diffusion of diethyl ether into a concentrated acetone solution of the complex. Single crystals of **3** were obtained by slow cooling a concentrated solution of the complex in hexanes. Single crystals of **4** were obtained by adding two drops of toluene to a concentrated hexane solution of the complex and slow cooling for three weeks. Single crystals of **5** and **6** were obtained by vapor diffusion of diethyl ether into a concentrated THF solution of the appropriate complex. Single-crystal X-ray diffraction data were collected with a Bruker Proteum diffractometer equipped with two CCD detectors (Apex2 and Platinum 135) sharing a common MicroStar microfocus Cu rotating anode generator running at 45 mA and 60 kV (Cu Kα = 1.54178 Å).

ASSOCIATED CONTENT

Supporting Information

NMR spectra and characterization of complexes and detailed information about performed simulations, reactivity, and X-ray crystallographic data (PDF)

Cartesian coordinates (XYZ)

Accession Codes

CCDC 2044718–2044719 and 2067363–2067366 contain the supplementary crystallographic data for compounds **1**–**6**. These data can be obtained free of charge via www.ccdc.cam.ac.uk/data_request/cif, or by emailing data_request@ccdc.cam.ac.uk, or by contacting The Cambridge Crystallographic Data Centre, 12 Union Road, Cambridge CB2 1EZ, UK; fax: +44 1223 336033.

AUTHOR INFORMATION

Corresponding Author

James D. Blakemore – *Department of Chemistry, University of Kansas, Lawrence, Kansas 66045, United States;* orcid.org/0000-0003-4172-7460; Phone: +1 (785) 864-3019; E-mail: blakemore@ku.edu

Authors

Chelsea G. Comadoll – *Department of Chemistry, University of Kansas, Lawrence, Kansas 66045, United States;* orcid.org/0000-0002-5273-7966

Wade C. Henke – *Department of Chemistry, University of Kansas, Lawrence, Kansas 66045, United States;* orcid.org/0000-0002-4574-8544

Julie A. Hopkins Leseberg – *Department of Chemistry, University of Kansas, Lawrence, Kansas 66045, United States;* orcid.org/0000-0001-6895-7333

Justin T. Douglas – *Molecular Structures Group, Nuclear Magnetic Resonance Laboratory, University of Kansas, Lawrence, Kansas 66045, United States;* orcid.org/0000-0002-7901-184X

Allen G. Oliver – *Department of Chemistry and Biochemistry, University of Notre Dame, Notre Dame, Indiana 46556, United States;* orcid.org/0000-0002-0511-1127

Victor W. Day – *Department of Chemistry, University of Kansas, Lawrence, Kansas 66045, United States*

Author Contributions

The manuscript was written through contributions of all authors. All authors have given approval of the final version of the manuscript.

Notes

The authors declare no competing financial interest.

ACKNOWLEDGMENT

The authors thank Sarah Neuenswander for assistance with NMR spectroscopy. This work was supported by the US National Science Foundation through award OIA-1833087. The authors also acknowledge the U.S. National Institutes of Health for support of the NMR instrumentation used in this study (Grants S10OD016360 and S10RR024664).

REFERENCES

[1] Kaesz, H. D.; Saillant, R. B., Hydride complexes of the transition metals. *Chem. Rev.* **1972,** *72*, 231-281.

[2] Rakowski Dubois, M.; Dubois, D. L., Development of Molecular Electrocatalysts for CO2 Reduction and H2 Production/Oxidation. *Accounts of Chemical Research* **2009,** *42*, 1974-1982.

[3] (a) Kölle, U.; Grätzel, M., Rhodium(III) complexes as homogeneous catalysts for the photoreduction of protons to hydrogen. *Angew. Chem.* **1987,** *99*, 572-574. (b) Kölle, U.; Grätzel, M., Organometallic Rhodium(III) Complexes as Catalysts for the Photoreduction of Protons to Hydrogen on Colloidal TiO_2. *Angew. Chem. Int. Ed. Engl.* **1987,** *26*, 567-570.

[4] (a) White, C.; Yates, A.; Maitlis, P. M., (η^5-Pentamethylcyclopentadienyl)Rhodium and -Iridium Compounds. *Inorg. Synth.* **1992,** *29*, 228-234. (b) Mantell, M. A.; Kampf, J. W.; Sanford, M., Improved Synthesis of $[Cp^RRhCl_2]_2$ Complexes. *Organometallics* **2018,** *37*, 3240-3242.

[5] (a) Peng, Y.; Ramos-Garcés, M. V.; Lionetti, D.; Blakemore, J. D., Structural and Electrochemical Consequences of [Cp*] Ligand Protonation. *Inorg. Chem.* **2017,** *56*, 10824-10831. (b) Henke, W. C.; Lionetti, D.; Moore, W. N. G.; Hopkins, J. A.; Day, V. W.; Blakemore, J. D., Ligand Substituents Govern the Efficiency and Mechanistic Path of Hydrogen Production with [Cp*Rh] Catalysts. *ChemSusChem* **2017,** *10*, 4589-4598.

[6] Kölle, U.; Kang, B. S.; Infelta, P.; Comte, P.; Grätzel, M., Electrochemical and pulse-radiolytic reduction of (pentamethylcyclopentadienyl)(polypyridyl)rhodium complexes. *Chem. Ber.* **1989,** *122*, 1869-1880.

[7] Ruppert, R.; Herrmann, S.; Steckhan, E., Very efficient reduction of $NAD(P)^+$ with formate catalysed by cationic rhodium complexes. *J. Chem. Soc., Chem. Commun.* **1988**, 1150-1151.

[8] Quintana, L. M. A.; Johnson, S. I.; Corona, S. L.; Villatoro, W.; Goddard, W. A.; Takase, M. K.; VanderVelde, D. G.; Winkler, J. R.; Gray, H. B.; Blakemore, J. D., Proton-hydride tautomerism in hydrogen evolution catalysis. *Proc. Nat. Acad. Sci. U.S.A.* **2016,** *113*, 6409-6414.

[9] (a) Steckhan, E.; Herrmann, S.; Ruppert, R.; Dietz, E.; Frede, M.; Spika, E., Analytical study of a series of substituted (2,2'-bipyridyl)(pentamethylcyclopentadienyl)rhodium and -iridium complexes with regard to their effectiveness as redox catalysts for the indirect electrochemical and chemical reduction of $NAD(P)^+$. *Organometallics* **1991,** *10*, 1568-1577. (b) Nam, D. H.; Park, C. B., Visible light-driven NADH regeneration sensitized by proflavine for biocatalysis. *Chembiochem* **2012,** *13*, 1278-1282.

[10] Pitman, C. L.; Finster, O. N. L.; Miller, A. J. M., Cyclopentadiene-mediated hydride transfer from rhodium complexes. *Chem. Commun.* **2016,** *52*, 9105-9108.

[11] Abura, T.; Ogo, S.; Watanabe, Y.; Fukuzumi, S., Isolation and Crystal Structure of a Water-Soluble Iridium Hydride: A Robust and Highly Active Catalyst for Acid-Catalyzed Transfer Hydrogenations of Carbonyl Compounds in Acidic Media. *J. Am. Chem. Soc.* **2003,** *125*, 4149-4154.

[12] Hopkins, J. A.; Lionetti, D.; Day, V. W.; Blakemore, J. D., Chemical and Electrochemical Properties of [Cp*Rh] Complexes Supported by a Hybrid Phosphine-Imine Ligand. *Organometallics* **2019,** *38*, 1300-1310.

[13] Boyd, E. A.; Lionetti, D.; Henke, W. C.; Day, V. W.; Blakemore, J. D., Preparation, Characterization, and Electrochemical Activation of a Model [Cp*Rh] Hydride. *Inorg. Chem.* **2019,** *58*, 3606-3615.

[14] Muckerman, J. T.; Skone, J. H.; Ning, M.; Wasada-Tsutsui, Y., Toward the accurate calculation of pKa values in water and acetonitrile. *Biochim. Biophys. Acta Bioenerg.* **2013,** *1827*, 882-891.

[15] (a) Klingert, B.; Werner, H., Basische Metalle, XLII. Die Metall-Basizität der Komplexe $C_5Me_5Rh(PMe_3)_2$, $C_5Me_5Rh(C_2H_4PMe_3$ und $C_5Me_5Rh(C_2H_4)P_2Me_4$: Neue Pentamethyl-cyclopentadienylrhodium(I)- und -rhodium(III)-Verbindungen. *Chem. Ber.* **1983,** *116*, 1450-1462. (b) Faller, J. W.; D'Alliessi, D. G., Tunable Stereoselective Hydrosilylation of PhC∶CH Catalyzed by Cp*Rh Complexes. *Organometallics* **2002,** *21*, 1743-1746.

[16] (a) Zhang, F.; Jia, J.; Dong, S.; Wang, W.; Tung, C.-H., Hydride Transfer from Iron(II) Hydride Compounds to $NAD(P)^+$ Analogues. *Organometallics* **2016,** *35*, 1151-1159. (b) Faraone, F.; Bruno, G.; Schiavo, S. L.; Tresoldi, G.; Bombieri, G., η^5-Cyclopentadienylrhodium(I) complexes containing diphosphines and their reactions with the electrophiles H^+ and Me^+. Crystal and molecular structure of $[Rh(\eta-C_5H_5)(CO)(Ph_2PCH_2PPh_2)]$, a complex with a unidentate bis(diphenylphosphino)methane ligand. *J. Chem. Soc., Dalton Trans.* **1983**, 433-438. (c) Castillo, C. E.; Stoll, T.; Sandroni, M.; Gueret, R.; Fortage, J.; Kayanuma, M.; Daniel, C.; Odobel, F.; Deronzier, A.; Collomb, M.-N., Electrochemical Generation and Spectroscopic Characterization of the Key Rhodium(III) Hydride Intermediates of Rhodium Poly(bipyridyl) H_2-Evolving Catalysts. *Inorg. Chem.* **2018,** *57*, 11225-11239. (d) Roy, S.; Sharma, B.; Pécaut, J.; Simon, P.; Fontecave, M.; Tran, P. D.; Derat, E.; Artero, V., Molecular Cobalt Complexes with Pendant Amines for Selective Electrocatalytic Reduction of Carbon Dioxide to Formic Acid. *J. Am. Chem. Soc.* **2017,** *139*, 3685-3696. (e) Elgrishi, N.; Kurtz, D. A.; Dempsey, J. L., Reaction Parameters Influencing Cobalt Hydride Formation Kinetics: Implications for Benchmarking H_2-Evolution Catalysts. *J. Am. Chem. Soc.* **2017,** *139*, 239-244.

[17] (a) Pal, S.; Kusumoto, S.; Nozaki, K., Dehydrogenation of Dimethylamine–Borane Catalyzed by Half-Sandwich Ir and Rh Complexes: Mechanism and the Role of Cp* Noninnocence. *Organometallics* **2018,** *37*, 906-914. (b) anerjee, S.; Soldevila-Barreda, J. J.; Wolny, J. A.; Wootton, C. A.; Habtemariam, A.; Romero-Canelón, I.; Chen, F.; Clarkson, G. J.; Prokes, I.; Song, L.; O'Connor, P. B.; Schünemann, V.; Sadler, P. J., New activation mechanism for half-sandwich organometallic anticancer complexes. *Chem. Sci.* **2018,** *9*, 3177-3185.

[18] (a) Ogata, K.; Seta, J.; Yamamoto, Y.; Kuge, K.; Tatsumi, K., One-pot syntheses of alkenyl-phosphonio complexes of ruthenium(II), rhodium(III) and iridium(III) bearing *p*-cymene or pentamethylcyclopentadienyl groups. *Inorganica Chim. Acta* **2007,** *360*, 3296-3303. (b) Tanase, T.; Yoshii, A.; Otaki, R.; Nakamae, K.; Mikita, Y.; Kure, B.; Nakajima, T., Synthesis and structures of dinuclear Rh^{III} and Ir^{III} complexes supported by a tetraphosphine, *meso*- or *rac*-bis{[(diphenylphosphinomethyl)phenyl]phosphino]}methane. *J. Organomet. Chem.* **2015,** *797*, 37-45.

[19] (a) Blakemore, J. D.; Hernandez, E. S.; Sattler, W.; Hunter, B. M.; Henling, L. M.; Brunschwig, B. S.; Gray, H. B., Pentamethylcyclopentadienyl rhodium complexes. *Polyhedron* **2014,** *84*, 14-18. (b) Nakai, H.; Jeong, K.; Matsumoto, T.; Ogo, S., Catalytic C–F Bond Hydrogenolysis of Fluoroaromatics by $[(\eta^5\text{-}C_5Me_5)RhI(2,2'\text{-bipyridine})]$. *Organometallics* **2014,** *33*, 4349-4352.

[20] Shannon, R. D., Revised effective ionic radii and systematic studies of interatomic distances in halides and chalcogenides. *Acta Cryst. A* **1976,** *32*, 751-767.

[21] Regarding the assignment of $^3J_{H,Rh}$ = 4.5 Hz and $^4J_{H,H}$ = 3.2 Hz for the downfield methylene proton: These coupling constants cannot be assigned concretely with inference from the appearance of the hydride resonances alone, due to broadness and the I = 1/2 nature of both H and Rh. The assignment of $^3J_{H,Rh}$ vs. $^4J_{H,H}$ is tentative, and based on the general assumption that a three-bond coupling should have a higher magnitude than a four-bond coupling. ^{103}Rh NMR could solidify this assignment, but such work is challenging due to the low gyromagnetic ratio of Rh.

[22] Shaka, A. J.; Keeler, J.; Freeman, R., Evaluation of a new broadband decoupling sequence: WALTZ-16. *J. Magn. Reson.* **1983,** *53*, 313-40.

[23] Shaka, A. J.; Keeler, J., Broadband spin decoupling in isotropic liquids. *Prog. Nucl. Magn. Reson. Spectrosc.* **1987,** *19*, 47-129.

[24] (a) Hoffman, R. A.; Forsén, S., High Resolution Nuclear Magnetic Double and Multiple Resonance. *Prog. NMR Spec.* **1966,** *1*, 15-204. (b) Cotton, F. A.; Marks, T. J., Interpretation of a Spin-Tickling Experiment on (Monohaptocyclopentadienyl)-(methyl)(dichloro)silane. *Inorg. Chem.* **1970,** *9*, 2802-2804.

[25] (a) Kupce, E.; Freeman, R.; Wider, G.; Wuethrich, K., Suppression of cycling sidebands using bi-level adiabatic decoupling. *J. Magn. Reson., Ser. A* **1996,** *122*, 81-84. (b) Weigelt, J.; Hammarstroem, A.; Bermel, W.; Otting, G., Removal of zero-quantum coherence in protein NMR spectra using SESAM decoupling and suppression of decoupling sidebands. *J. Magn. Reson., Ser. B* **1996,** *110*, 219-224. (c) Tenailleau, E.; Akoka, S., Adiabatic ^{1}H decoupling scheme for very accurate intensity measurements in ^{13}C NMR. *J. Magn. Reson.* **2007,** *185*, 50-58.

[26] Appel, A. M.; Helm, M. L., Determining the Overpotential for a Molecular Electrocatalyst. *ACS Catal.* **2014,** *4*, 630-633.

[27] (a) Akitt, J. W.; Mann, B. E., *NMR and Chemistry: An Introduction to Modern NMR Spectroscopy*, CRC Press, 2000, 4th edn. (b) Harris, R. K., *Nuclear Magnetic Resonance Spectroscopy: A Physicochemical View*, Pearson Education, 1986.

[28] Stevenson, P. J., Second-order NMR spectra at high field of common organic functional groups. *Org. Biomol. Chem.* **2011,** *9*, 2078-2084.

[29] Willcott, M. R., MestRe Nova. *J. Am. Chem. Soc.* **2009,** *131*, 13180-13180.

[30] Bernstein, H. J.; Pople, J. A.; Schneider, W. G., Analysis of Nuclear Magnetic Resonance Spectra. I. Systems of Two and Three Nuclei. *Can. J. Chem.* **1957,** *35*, 65-81.

[31] Regarding the reasoning behind indicated Pople notation: Because of the complexity of the spin system in complexes **1** and **5**, the authors simply aim to use Pople notation as a guide to explain the nuclei involved. The A and B notations were chosen for the methylene protons because they are geminal, inequivalent nuclei. The Cp* methyl protons were denoted as M to indicate distance between the methylene protons and the methyl protons in the spectrum, moving upfield. Y and Z denote phosphorus and rhodium, respectively, because these two nuclei are not present in the ^{1}H NMR spectrum. For **5**, the hydride ligand was denoted as X to indicate even further separation upfield from the Cp* methyl protons, inserted in front of phosphorus and rhodium symbols because it does appear in the spectrum.

[32] Redfield, C., "Proteins Studied by NMR" in *Encyclopedia of Spectroscopy and Spectrometry*, Lindon, J. C.; Tranter, G. E.; Koppenaal, D. W., Eds. Academic Press: Oxford, 2017; 3rd edn., pp 759-765.

[33] Fulmer, G. R.; Miller, A. J. M.; Sherden, N. H.; Gottlieb, H. E.; Nudelman, A.; Stoltz, B. M.; Bercaw, J. E.; Goldberg, K. I., NMR Chemical Shifts of Trace Impurities: Common Laboratory Solvents, Organics, and Gases in Deuterated Solvents Relevant to the Organometallic Chemist. *Organometallics* **2010,** *29*, 2176-2179.

[34] Harris, R. K.; Becker, E. D.; Cabral De Menezes, S. M.; Goodfellow, R.; Granger, P., NMR nomenclature: Nuclear spin properties and conventions for chemical shifts (IUPAC recommendations 2001). *Concepts Magn. Reson.* **2002,** *14*, 326-346.

[35] Harris, R. K.; Becker, E. D.; De fMenezes, S. M. C.; Granger, P.; Hoffman, R. E.; Zilm, K. W., Further Conventions for NMR Shielding and Chemical Shifts. *IUPAC Standards Online* **2016**, *80*, 59-84.

For Table of Contents Only:

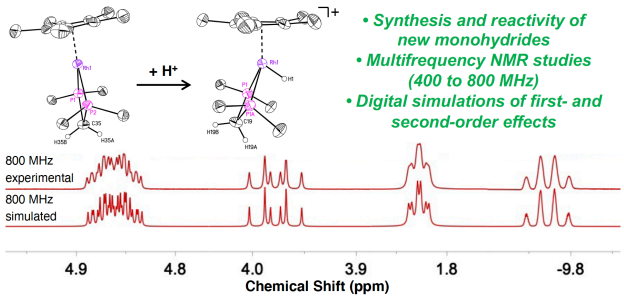

TOC Synopsis: A sequential reduction/protonation strategy has been used to prepare two new [Cp*Rh] monohydrides supported by the diphosphine ligands dppm and Xantphos. Multifrequency NMR data (400–800 MHz) and comprehensive digital simulations have been used to map complex magnetic coupling networks in two of the dppm compounds that feature diastereotopic methylene protons.